RSC Advances

PAPER

View Article Online
View Journal | View Issue

Cite this: *RSC Adv.*, 2024, **14**, 31243

Novel environmental applications of green tea: sensing and remediation of Ag^+ in aqueous system†

Ankita Doi,[a] Mainak Ganguly *[b] and Priyanka Sharma[b]

Received 31st July 2024
Accepted 24th September 2024

DOI: 10.1039/d4ra05545d

rsc.li/rsc-advances

The strong fluorescence of green tea was quenched with Fe^{3+} because of ligand-to-metal charge transfer and subsequent formation of magnetite (Fe_3O_4) nanoparticles (heavy metal effect). Ag^+ restored the lost fluorescence by confining iron particles (capped with Cl^-) with the formation of AgCl. Thus, toxic Ag was sensed in the aqueous system with a linear detection range of 10^{-4} M to 10^{-7} M and a detection limit of 4.1×10^{-9} M. The sensing protocol was applied for natural samples to detect Ag^+. Gallic acid was found to be the pivotal component in the tea extract used to design a sensing platform. The company of the green tea were also varied and obtained comparable results.

Introduction

Silver ions have a significant role in the metabolism of copper. Ag^+ plays an important role in the glycolysis process for pyruvate and lactate formation. Silver ions have been known for their antibacterial activities since ancient times; hence the silver vessels are often used to hoard liquids or water to prevent it from any microbial infection. Ions of silver with micromolar concentrations (1 to 10 μM) are adequate to destroy bacteria in water.[1,2] Salts of Ag such as $AgNO_3$ are used in medicine, pharmacology, the electric industry, *etc.* Earlier silver nitrate and iodide were used in black and white photography.[3] Ag^+ and Ag nanoparticles (colloidal silver) are well-used in nanotechnology. It was reported that 10 ppm (10 mg L^{-1}) of the quantity of silver has 90% of the Ag^+ ions and only 10% Ag NPs.[4] Some studies showed that silver ions have better antibacterial activity than AgNPs. It was reported that AgNPs produce Ag^+ ions.[1]

However, pollution due to industries is a matter of great concern all over the world. Pollution due to heavy metals is one of them. Not only industrial waste but also electronic waste, which kept on piling, emerged heavy metals from semiconductors and batteries. Among these metals, silver is one of them polluting the soil[5] and water sources due to leaching. Silver ions and nanoparticles are found to be quite toxic. Depending on the doses and size, Ag has been proven to be toxic to bacteria,[6] yeast, algae,[7] crustaceans,[8] and humans. They can cause alterations in the enzymes of the liver, levels of neurotransmitters, loss in weight, lethargy, or even death.[9] Thus, Ag^+ sensing was an active field of research. Mehta *et al.* and Sharma *et al.* summarized the sensing of Ag^+ employing various existing methods.[10,11]

Green tea (GTE) is a well-known beverage in our daily life. It is also used in cosmetics,[12] food,[13] traditional medicines[14] *etc.* However, in the synthesis of the nanoparticles, its use is growing day by day, because of the reducing and stabilizing properties of the polyphenols of GTE. Gottimukkala and Hao *et al.* reported the synthesis of iron nanoparticles using GTE, which is black and has a zero oxidation state of iron.[15] Plachtová *et al.* synthesized iron and iron-oxide nanoparticles for the elimination of malachite green dye from water along with ecotoxicology.[16]

Iron-based nanoparticles are widely used for environmental remediation, *e.g.*, toxic dye removals, removal of heavy metals, *etc.*[10] due to electrostatic attraction, hydrogen bonding, *etc.* However, in recent times food sources are also used in fluorescence to detect pollutants such as heavy metals, *etc.* Reversibly, different nanoparticles are used for the detection of components of food sources.[17] He *et al.* used green tea carbon dots for Fe^{3+} detection.[18] Similarly, Patra *et al.* used green tea carbon dots for chromium(VI) detection.[19]

Conversely, ionic metals such as Cu^{2+} are used for fluorescence ionic probe formation and detection of herbicides such as glyphosate in green tea.[20] Sequentially, components of green tea such as tannic acid used for the synthesis of Fe_3O_4-based ethanol sensing.[21]

However, iron nanoparticles for sensing applications have not been available in the literature. In the present work, Ag^+ sensing selectively and sensitively employing iron hydrosol, passivated with green tea (GTEFe) fluorometrically is demonstrated for the first time. No report is so far available for the fluorometric use of green tea and iron hydrosol with environmental applications. The sensing of Ag^+ was also compared with different groups (Table S1, ESI†).

[a]*Department of Biosciences, Manipal University Jaipur, Jaipur, 303007, Rajasthan, India*

[b]*Department of Chemistry, Manipal University Jaipur, Jaipur, 303007, Rajasthan, India. E-mail: mainak.ganguly@jaipur.manipal.edu*

† Electronic supplementary information (ESI) available. See DOI: https://doi.org/10.1039/d4ra05545d

Results and discussion

Green tea extract (GTE)

Green tea has polyphenols, which incorporate phenolic acids, flavonoids, flavanols, flavandiols, and flavonoids. These compounds might tally up to 30% of total dry weight. Out of total green tea polyphenols (GTPs), the majority of them are flavonols, normally regarded as catechins. In addition, there are phenolic acids such as gallic acids and distinguishing amino acids like theanine.

Most goods made from green tea are extracts, either liquid or powder, with varying percentages of polyphenols (45–90%) and caffeine (0.4–10%). Epigallocatechin, epicatechin, EGCG, and epicatechin-3-gallate are the four primary types of catechins found in green tea.[22]

Various components are present in GTE. The colour of the GTE is greenish-yellow. The GTE extract was stored at 4 °C in the refrigerator for further usage. The GTE showed good fluorescence $\lambda_{ex} = 274$ and $\lambda_{max} = 400$ nm. The UV-Vis $\lambda_{ex} = 274$ nm [Fig. 1].

GTEFe hydrosol

Fe_3O_4 nanoparticles (black hydrosol, GTEFe) were synthesized from green tea extract, made *via* submerging 250 mg green tea leaves (Symphony) for 10 h at room temperature (25 °C) and filtered through a Whatman filter paper. The procedure was green and energetically favourable. The green tea extract (GTE) was greenish-yellow in colour. No heat or external energy was supplied to obtain the extract. Moreover, our synthetic protocol was simple, one pot, and cost-effective. Synthesized Fe_3O_4 nanoparticles were non-magnetic, evident from using a powerful magnet (Scheme 1).

Sensing of Ag^+

After the addition of the Fe^{3+}, the fluorescence was strongly quenched with the formation of GTEFe at λ_{em} 400 nm. Such quenched fluorescence was restored after the addition of Ag^+ in GTEFe to form AgGTEFe (λ_{em} 460 nm). Ag^+-induced fluorescence enhancement was quite selective and sensitive. Other metal ions *in lieu* of Ag^+ (Hg^{2+}, Ba^{2+}, Cu^{2+}, Ni^{2+}, Na^+, Ca^{2+}, Al^{3+}, Fe^{3+}, K^+, Cr^{3+} and Zn^{2+}) were used. However, no enhancement was observed for other metal ions, unlike Ag^+ (Fig. 2 and S1, ESI†). We also performed chloroauric acid *in lieu* of silver nitrate. However, fluorescence enhancement was observed for silver only. The blue shift for GTE was 67 nm for GTEFe and the red shift of 116 nm for AgGTEFe. Increased stroke shift was associated with increased selectivity of the analytes. Tunable stokes shifts warrant novel fluorescent probes for accuracy and precision in sensing for the upcoming generation applications.[23] From the absorption spectra, it was observed that the λ_{max} of GTE at 274 nm was blue shifted (λ_{max} 270 nm) in GTEFe and further blue shifted (λ_{max} 264 nm) in AgGTEFe with hypsochromic shift (Fig. S2, ESI†). Not only enhancement of fluorescence was observed by Ag^+ in GTEFe, but also the highest absorbance at λ_{max} 264 nm was noticed with Ag^+ (in comparison to the addition of other metal ions) (Fig. S3, ESI†). The quantum yield for the GTE hydrosol was 1.68%, while the quantum yield for AgGTEFe was 2.02%.

This proposed sensing platform was also compared with other reported platforms (Table S1, ESI†).

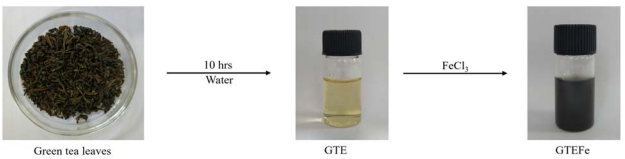

Scheme 1 Schematic representation for the formation of GTEFe.

Sensitivity

Not only selectivity but also sensitivity is a vital factor for sensing applications. A monotonous increase of fluorescence in the range of 10^{-7} M to 10^{-3} M of $[Ag^+]$ was found. When $[Ag^+] > 10^{-3}$ M, a decrease in fluorescence was observed due to the heavy metal effect.[24–26] At 10^{-2} M of $[Ag^+]$, the different signatures of the fluorescence spectrum were observed with quenched fluorescence intensity. A linear detection range, 10^{-4} M to 10^{-7} M by plotting fluorescence intensity *vs.* $[Ag^+]$ with a limit of detection (LOD) of 4.1×10^{-9} M was observed. I_0 and I were fluorescence intensity before and after Ag^+ treatment on GTEFe, respectively (Fig. 3). The absorbance at λ_{max} 264 nm was increased gradually with increased $[Ag^+]$ in AgGTEFe (Fig. S5, ESI†). Silver nitrate is the only commonly available salt that is soluble in water. We added sodium salts with different counter anions in AgGTEFe and different extent of fluorescence was observed as in Fig. S6, ESI.†

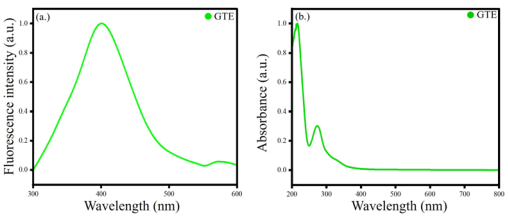

Fig. 1 (a) Fluorescence spectra of GTE; (b) UV-Vis absorbance of GTE.

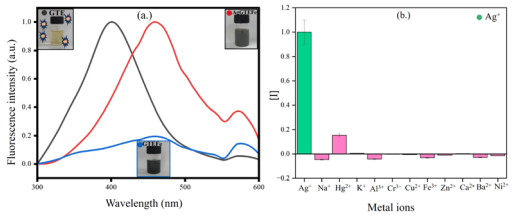

Fig. 2 (a) Fluorescence spectra of GTE, GTEFe, AgGTEFe; (b) bar diagram regarding [I] of GTEFe in the presence of different metal ions; $[Ag^+] = 10^{-3}$ M.

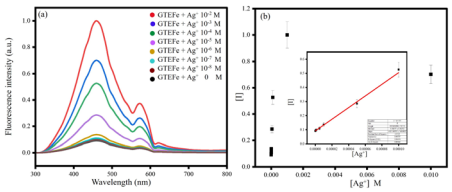

Fig. 3 (a) Fluorescence spectra of GTE at different [Ag^+]; (b) plot of [I] *vs.* [Ag^+] and linear detection range of Ag^+ detection (inset).

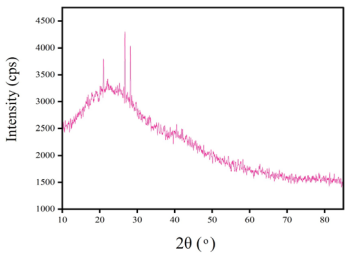

Fig. 5 XRD pattern of GTEFe.

Effect of pH

pH has a significant role in the emissive behaviour of GTEFe in the presence of Ag^+. GTEFe (as mentioned in the Experimental section) had a pH of 4. Then titration of Ag^+ was performed (Fig. 2). GTEFe at pH 2, 6, 8, 10, and 12 was made. pH was adjusted with dilute HCl and NaOH solution. No buffer was introduced with GTEFe. pH 4 had maximum enhancement with Ag^+. The order of fluorescence intensities is as follows, pH 4 > pH 2 > pH 6 = pH 8 > pH 10 > pH 12. Higher pH produced AgOH,[27] hindering the binding with Fe to display low fluorescence (Fig. 4). The fluorescence of AgGTEFe was maximum at pH 4. At higher pH, fluorescence decreased due to the formation of AgOH. As mentioned in the mechanism section, the fluorescence enhancement was related to the formation of AgCl. Thus, AgCl formation was hindered at higher pH. At strongly acidic pH also fluorescence enhancement was low the due to protonation of polyphenols in GTE.

Characterisation

The XRD spectra lacked characteristic diffraction peaks which indicated that the GTEFe nanoparticles were amorphous by nature.[28,29] The broad peak at 2θ in between 20° and 30° corresponded to covered organic materials from the reaction, which were responsible for stabilizing the synthesized Fe particles (Fig. 5).[28]

The FTIR spectrum of the GTEFe nanoparticles exposed the estimated bands of ν(Fe–OH) and ν(Fe–O). The band at 624 cm^{-1} corresponds to the vibration of the Fe–O bond whereas 1621 and 3196 cm^{-1} bands represent ν(Fe–OH). The ν(Fe–O) band represents the presence of magnetite (Fig. 6).[30]

Particles were spheroids with a diameter of ~70 nm, observed from FESEM images (Fig. 7).

TEM image indicated approximately 50 nm spherical particles (Fig. 8).

The oxidation states of silver and iron in AgGTEFe were investigated. In this regard, XPS (Fig. 9) and XRD (S5, ESI†) were analysed. From XPS analysis, it was observed that in AgGTEFe, Ag was at +1 oxidation state. Binding energies of 367.3 eV and 373.7 eV corresponded to Ag(I)$3d_{5/2}$ and Ag(I)$3d_{3/2}$, respectively.[31,32] The XPS peak of iron is comparatively broad due to the presence of Fe^{3+} and Fe^{2+}. Binding energy 710.1 eV was due to Fe(II)$2p_{3/2}$ while binding energy 711.4 eV was due to Fe(III)$2p_{3/2}$.[33,34] However, the peak of Fe(III)$2p_{1/2}$ was not prominent for AgGTEFe in the presence of ionic silver. XRD patterns also had parity with XPS data. The 2θ values 38°, 44°, 64° and 77° corroborated (111), (200), (210), (311) of Ag_2O, respectively.[35–37] Magnetite is an inverse spinel mixed metal oxide consisting of Fe^{2+}, Fe^{3+}, and O^2.[38] The broad XRD 2θ peak around 20° to 30° corresponded amorphous nature of iron and 2θ 29.4° indicated (220) planes of magnetite (Fig. S5, ESI†).[39,40] Thus, XRD and XPS analyses confirmed the presence of Fe_3O_4 and Ag_2O. The particles in AgGTEFe were magnetic, attracted by a strong magnet (unlike GTEFe). So, the FESEM of the sample could not be obtained FESEM due to its magnetic nature. It is more likely that zero-valent iron nanoparticles in the hydrosol of AgGTEFe were converted to iron oxide during the sample preparation (washing and drying) of XRD and XPS.

DLS of freshly prepared GTEFe after 30 min of sonication was performed. The 100% particles of GTEFe were with particle size 410.9 nm ± 147.8 nm. Similarly, DLS of freshly prepared AgGTEFe after 30 min of sonication. The 86.5% particles of AgGTEFe had a particle size of 242.1 ± 72.08 nm and 13.5% particles of AgGTEFe had a particle size of 10 774 ± 2461 nm. Both Ostwald ripening and digestive ripening were driving forces for the final size (Fig. S7, ESI†).[41,42]

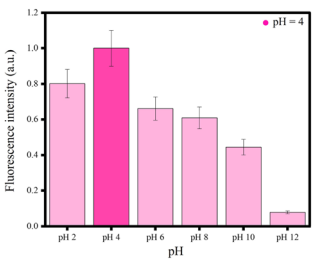

Fig. 4 AgGTEFe at different pHs.

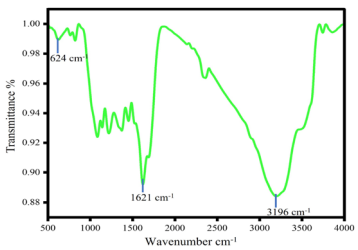

Fig. 6 FTIR spectrum of iron oxide (Fe_3O_4) nanoparticles.

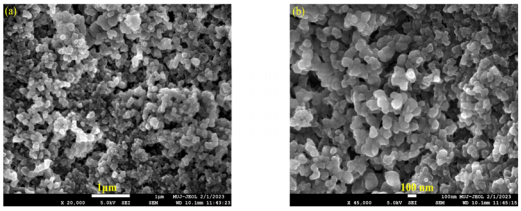

Fig. 7 FESEM of GTEFe at (a) low resolution and (b) high resolution.

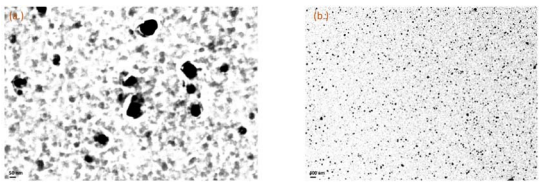

Fig. 8 TEM of GTEFe at (a) high resolution and (b) low resolution.

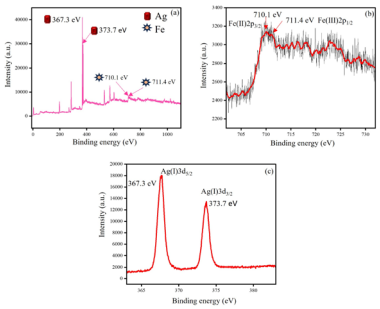

Fig. 9 XPS of AgGTEFe (a) wide angle, (b) Fe and (c) Ag.

The stability of GTEFe hydrosol was not great. A zeta potential of 4.8 mV indicated that the synthesized nanoparticles were passivated by the negatively charged capping agent of tea extract (oxidized form of polyphenol). On the contrary, AgGTEFe formed a precipitate with zeta potential 0 mV. Keeping this idea in mind, GTEFe as a nanotrap was designed to remove Ag^+ from water. Two pieces of cotton of equal mass (0.5 g) were taken. One piece of cotton wool was dipped in 10 mL GTEFe and dried in air. GTEFe-impregnated cotton wool was put inside the funnel. The 10^{-3} M Ag^+ solution was passed through unmodified and modified cotton wool separately. Unmodified cotton wool showed no significant change in the concentration of Ag^+. However, modified cotton wool trapped Ag^+ and the filtrate had a concentration 40 times lower (2.5×10^{-5} M) (Fig. 10).

The polyphenol present in the GTE could form a complex with Fe^{3+} resulting in fluorescence quenching in GTEFe due to charge transfer from ligand to metal.[43] After that, Fe^{3+} was reduced to Fe^0 (and subsequently converted to Fe_3O_4 due to aerial oxidation) and fluorescence quenching was observed due to the heavy metal effect.[25,26,44]

Mechanism

The inherent emissive property of GTE was lost with the addition of Fe^{3+}. As Fe^{3+} itself has absorbance, the addition of Fe^{3+}

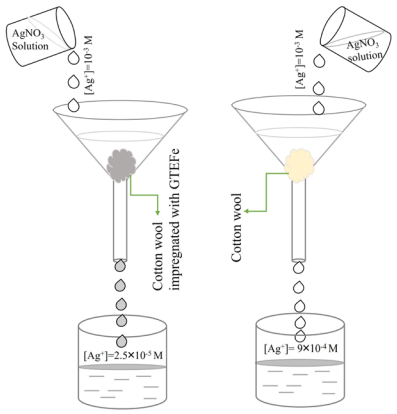

Fig. 10 Removal of $[Ag^+]$ *via* cotton wool with and without the impregnation of GTEFe.

might prevent the emission of the fluorescence.[45,46] The added Fe^{3+} was converted to Fe^0 and iron oxide[47,48] With fluorescence quenching due to the heavy metal effect.[24–26]

When Fe^{3+} was added to GTE, the fluorescence was remarkably quenched due to the absorption of energy by the ionic iron. Liu *et al.* illustrated the fluorescence quenching of the fluorophore *via* heavy metal ions with the absorption of energy of electronic transition (from conduction band to valence band).[49]

However, GTE contains polyphenols with reducing and stabilizing properties.[50] GTE reduced Fe and formed GTE-passivated Fe_3O_4 nanoparticles. As a corollary, polyphenols in GTE were converted to their quinone form. From UV-Vis spectroscopy, it was observed that the absorption peaks of GTE and GTEFe were overlapped, indicating the chance of non-radiating energy transfer from GTE to Fe_3O_4 nanoparticles and quenching was observed.

The RP (radiating plasmon) model states that the metal structures's optical properties can be computed *via* Mie theory, electrodynamics, and/or Maxwell's equations. The metal colloids's extinction might result from either scattering or absorption, depending on the size, form of the particle, and Mie theory. The model predicted that nanoparticles often extinguish fluorescence as absorption predominates over scattering. Consideringly, it was implied that the "lossy surface waves" that cause the quenching of fluorescence generated electron oscillations that were unable to emit to the far field due to the impossibility of wavevector matching.[51,52] In our present study, the emission from GTE in the proximity of Fe_3O_4 nanoparticles (*in situ* generated) became trapped plasmons, producing "lossy surface waves" and quenching of fluorescence was observed.

To understand further the mechanism of Ag^+ adsorption with GTEFe, GTEFe was synthesized with $Fe(NO_3)_3 \cdot 9H_2O$ *in lieu* of $FeCl_3$. The restoration of fluorescence after the addition of Ag^+ was also observed with GTEFe, synthesized from ferric nitrate. The fluorescence enhancement was low, and the spectral nature was broad. GTEFe (synthesized from $FeCl_3$), being passivated with Cl^-, produced AgCl, highly insoluble (1.6 ×

10^{-10} at 25 °C) with making precipitate. Fe^0 (produced *in situ* in the presence of GTE extract) also coagulated and settled down rendering GTE free to fluoresce. However, the unreacted metal ions present in the solution were attributed to be responsible for the red shift of the fluorescence. The increase of fluorescence of AgGTEFe [involving $Fe(NO_3)_3 \cdot 9H_2O$] with the addition of NaCl from outside further supported the role of Cl^- on fluorescence enhancement. It is to be noted that chloride has the lowest quenching ability than bromide and iodide. That is why fluorescence restoration was not influenced due to the presence of Cl^- ions.[53]

However, it was not the sole mechanism for fluorescence restoration, as GTEFe [synthesized from $Fe(NO_3)_3 \cdot 9H_2O$)] also showed somewhat fluorescence restoration. Ag^+ might also bind to zero-valent iron and the drift of electron density from Fe^0 to Ag^+ might be the driving force of Ag^+–Fe^0 interaction, as Fe^{3+} is the most stable form of iron. As a result, the quenching effect was decreased with AgGTEFe.

GTE is used by many researchers for the synthesis of nanoparticles due to its antioxidant properties. Though green tea is a natural product containing several compounds,[54] Vilchis-Nestor *et al.* demonstrated that gallic acid is the main compound for the antioxidant properties of green tea.[55] To understand the mechanism better the experiment was repeated with an aqueous solution of pure gallic acid instead of GTE. Similar fluorometric behaviour was observed for gallic acid like GTE. In other words, the fluorescence was quenched with the addition of Fe and restored with the addition of Ag^+ [Fig. S8, ESI†].

Muthusamy *et al.* demonstrated the formation of zero-valent metal nanoparticles from metal ion precursors by employing gallic acid. Gallic acid, as a corollary, was converted to *O*-quinone and capped synthesized nanoparticles.[56]

To be noted that GTE did not exhibit emissive behaviour with Ag^+. So, restoration of fluorescence was the driving factor for fluorescence enhancement (Fig. S9, ESI†).

The process was repeated by producing tea extract obtained from the LIPTON company. The quenching for GTEFe and enhancement for AgGTEFe. So, the trends of the fluorescence behaviour were similar for GTE obtained from Symphony and LIPTON (Fig. S10, ESI†).

Effect of temperature

The fluorescence behaviour of AgGTEFe was gauged at different temperatures after ageing AgGTEFe at different temperatures for 30 min. At low temperatures (10 °C) fluorescence was increased in comparison to room temperature due to decreased Brownian motion.[57] Slow increment of temperature generated a competition between increased Brownian motion and the interaction between Ag^+ & GTEFe. The first factor decreased fluorescence intensity, while the second factor increased fluorescence intensity. Thus, there were no significant changes in fluorescence behaviour from 20 °C to 50 °C (concerning room temperature 30 °C). From 60 °C, fluorescence was increased and at 70 °C, the highest increment was observed. This was because of the higher Ag^+ and Fe interaction, rendering GTE free.

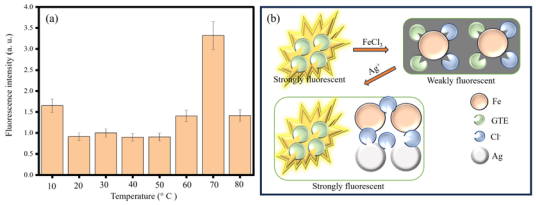

Fig. 11 Plot of I_T/I_{RT} at different temperatures, (b) schematic representation of restoration of fluorescence with Ag^+.

Further increase in temperature caused a huge increase in Brownian motion (Fig. 11).

Real water analysis

Natural water samples were gathered from multiple sources, such as the Yamuna River in Mathura, India, rain, tap and drinking water from Jaipur.

Varying quantities of Ag^+ were added to the water. The above-discussed fluorometric sensing techniques were used for Ag^+ detection in natural water. The obtained data showed that the actual spiked concentrations were quite close to the estimated data.

Adsorption of Ag^+ on GTEFe

For analyzing the efficacy of GTEFe in the removal of Ag^+ from solution and the nature of adsorption, various adsorption isotherms were fitted with the obtained data. Langmuir adsorption isotherm indicates homogenous sites of adsorption and monolayer of adsorbate on the adsorbent following the following equation.

$$\frac{C_e}{q_e} = \frac{1}{K_L Q_m} + \frac{C_e}{Q_m} \quad (1)$$

C_e indicates the equilibrium concentration of the Ag^+ (mg L^{-1}), whereas q_e denotes the adsorbed Ag^+ on the adsorbent GTEFe (mg g^{-1}). K_L denotes the Langmuir constant. Q_m is the maximum adsorption capacity calculated *via* slope obtained through straight line fitting of C_e/q_e *vs.* C_e. Freundlich adsorption isotherm establishes the empirical relation between heterogeneous sites of adsorption of GTEFe.

$$\log(q_e) = \log(K_F) + \frac{1}{n}\log(C_e) \quad (2)$$

A straight line slope, established among $\log(q_e)$ and $\log(C_e)$, provides the intensity of adsorption $1/n$. K_F denotes Freudlich constant. Multilayered adsorption explanation is provided by Elovich adsorption isotherm.

$$\ln\left(\frac{q_e}{C_e}\right) = -\frac{q_e}{Q_m} + \ln(K_E Q_m) \quad (3)$$

Maximum adsorption capacity (Q_m) for Langmuir adsorption isotherm was 2.24 mg g^{-1}. The coefficient of determination, R^2 value came out to be 0.981. However, R^2 values for Freundlich

and Elovich were 0.883 and 0.948, respectively. The R^2 value for Elovich came closer to the R^2 value of the Langmuir plot. However, the best-fitted R^2 determined that Ag forms a monolayer on the adsorbent GTEFe. Langmuir adsorption isotherm traits are better understood by dimensionless constant R_L.

$$R_L = \frac{1}{1 + K_L C_0} \quad (4)$$

Here, C_0 is the maximum preliminary concentration (mg L^{-1}), and K_L is the Langmuir constant. R_L describes the kind of isotherm which can be unfavourable ($R_L > 1$), favourable ($0 < R_L < 1$), or linear ($R_L = 1$). For GTEFe and Ag adsorption isotherm, the absolute values of R_L and K_L were found to be 0.0672 and 0.02056 respectively indicating favorable adsorption (Fig. 12).

Experimental

Materials and instruments

The chemicals used in this study were of analytical calibre. In the entire study, distilled water was utilized. Glassware was washed using newly prepared aqua regia then soap-water and with plenty of distilled water. Glassware was completely dried before utilisation. Green tea was of Tea City Symphony (brand) with licence number 10013031000840. Green tea was purchased from a supermarket in Jaipur, Rajasthan. All metal salts including $FeCl_3$ were procured from Sigma Aldrich except $AgNO_3$. $AgNO_3$ was purchased by Merck Specialities Private Limited respectively. Whatman paper of Whatman™ Cat no 1001 125 was used. To analyse fluorescence at room temperature Horiba FluoroMax-4 spectrometer was utilized. For FESEM, JEOL Make JSM-7610FPlus FESEM at SAIF, a high resolution (1 kV 1.0 nm, 15 kV 0.8 nm) was used. For XRD analyses, Rigaku makes an automated multipurpose X-ray Diffractometer (model: SMARTLAB) was utilized. Omicron ESCA (Electron Spectroscope for Chemical Analysis), Oxford Instrument Germany (resolution 0.60 eV) used for XPS. Model-FEI Tecnai G2 20 was used for TEM.

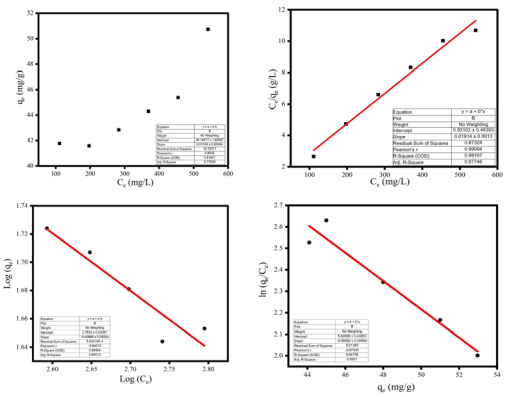

Fig. 12 (a) Plot q_e *vs.* C_e (b) Langmuir (c) Freundlich (d) Elovich isotherms for Ag^+ adsorption on GTEFe.

Synthesis of GTE

Green tea (1 g) was soaked in 100 mL of distilled water for 10 h. After 10 h, the formed extract was filtered with the Whatman paper. The filtrate (extract) was stored at 4 °C and the used leaves were discarded.

Synthesis of GTEFe

The 39 mL of freshly prepared green tea extract was put into a beaker and 13 mL of $FeCl_3$ (6.1×10^{-2} M) solution was added into it (ratio 3 : 1). A black colour hydrosol (GTEFe) was formed.

Error analysis

All the experiments were performed thrice independently, and the error bar was calculated from the standard deviation of the obtained data.

Conclusions

For the first time, green tea extract produced at room temperature was used as a sensing platform for water contaminants. The selectivity and sensitivity of the Ag^+ detection for prototype applications are promising. The sensing platform was energetically favourable and cost-effective. This research will open up a new window for the scientist venturing into the field of material chemistry and environmental nanoscience. A highly used beverage has been utilized here for the first time for environmental remediation. More research is warranted to understand the effects of various components inside the tea extract for making a fluorescence platform.

Data availability statement

All the data are included in ESI.†

Conflicts of interest

There are no conflicts to declare.

Acknowledgements

The authors are thankful to CSIR (Council of Scientific & Industrial Research) for financial assistance, SAIF (MUJ) and CAF (MUJ) for providing instrumental facilities.

Notes and references

1 A. Hamad, K. S. Khashan and A. Hadi, *J. Inorg. Organomet. Polym. Mater.*, 2020, **30**, 4811–4828.
2 S. Paul, P. Barman, N. Dey and M. Watkinson, *Sens. Diagn.*, 2024, **3**, 946–967.
3 B. Tepla, K. Demnerova and H. Stiborova, *J. Cult. Herit.*, 2020, **44**, 218–228.
4 J. R. Swathy, M. Udhaya Sankar, A. Chaudhary, S. Aigal, Anshup and T. Pradeep, *Sci. Rep.*, 2014, **4**, 7161.

5 S. I. Kolesnikov, N. I. Tsepina, L. V. Sudina, T. V. Minnikova, K. S. Kazeev and Y. V. Akimenko, *Appl. Environ. Soil Sci.*, 2020, **2020**, 9.
6 Y. Choi, H. A. Kim, K. W. Kim and B. T. Lee, *J. Environ. Sci.*, 2018, **66**, 50–60.
7 I. Moreno-Garrido, S. Pérez and J. Blasco, *Mar. Environ. Res.*, 2015, **111**, 60–73.
8 A. Ivask, I. Kurvet, K. Kasemets, I. Blinova, V. Aruoja, S. Suppi, H. Vija, A. Kakinen, T. Titma, M. Heinlaan, M. Visnapuu, D. Koller, V. Kisand and A. Kahru, *PLoS One*, 2014, **9**, 14.
9 N. Hadrup and H. R. Lam, *Regul. Toxicol. Pharmacol.*, 2014, **68**, 1–7.
10 P. K. Mehta, L. N. Neupane, S. H. Park and K. H. Lee, *J. Hazard. Mater.*, 2021, **411**, 125041.
11 P. Sharma, M. Ganguly and A. Doi, *Appl. Nanosci.*, 2024, 1–13.
12 Y. Q. Xu, S. Q. Chen, H. B. Yuan, P. Tang and J. F. Yin, *J. Food Sci. Technol.*, 2012, **49**, 362–367.
13 Q. V. Vuong, C. E. Stathopoulos, M. H. Nguyen, J. B. Golding and P. D. Roach, *Food Rev. Int.*, 2011, **27**, 227–247.
14 V. V Chopade, A. A. Phatak, A. B. Upaganlawar and A. A. Tankar, *Pharmacogn. Rev.*, 2008, **2**, 157–162.
15 D. Z. Gottimukkala and P. Harika Reddy, *J. Nanomed. Biother. Discovery*, 2017, **7**, 1–4.
16 P. Plachtová, Z. Med, R. Zbo, R. S. Varma and B. Maršálek, *ACS Sustain. Chem. Eng. Iron*, 2018, **6**, 8679–8687.
17 A. Kushwaha, G. Singh, U. K. Gaur and M. Sharma, *Mater. Adv.*, 2024, **5**, 4378–4400.
18 Y. He, S. Liu, F. Xie, Y. Zhou and X. Yang, *J. Food Compos. Anal.*, 2024, **132**, 106332.
19 P. Swagata, A. K. Golder and R. V. S. Uppaluri, *Opt. Mater.*, 2024, **154**, 115767.
20 C. Siying, Z. Yiwan, S. Xinxiang, P. Xiutan, F. Haiyan and S. Yuanbin, *Food Chem.*, 2004, **447**, 138859.
21 S. Ananthi, M. Kavitha, E. R. Kumar, A. Balamurugan, Y. Al-Douri, H. K. Alzahrani, A. A. Keshk, T. M. Habeebullah, H. Abdel-Hafez Shams and N. M. El-Metwaly, *Sensor. Actuator. B Chem.*, 2024, **352**, 131071.
22 S. M. Chacko, P. T. Thambi, R. Kuttan and I. Nishigaki, *China's Med.*, 2010, **5**, 1–9.
23 T. B. Ren, W. Xu, W. Zhang, X. X. Zhang, Z. Y. Wang, Z. Xiang, L. Yuan and X. B. Zhang, *J. Am. Chem. Soc.*, 2018, **140**, 7716–7722.
24 S. S. Tan, S. J. Kim and E. T. Kool, *J. Am. Chem. Soc.*, 2011, **133**, 2664–2671.
25 A. Sekar, R. Yadav and N. Basavaraj, *New J. Chem.*, 2021, **45**, 2326–2360.
26 I. K. Kandela and R. M. Albrecht, *Scanning*, 2007, **29**, 152–161.
27 I. E. Layla Badr, *Chem. Phys. Lett.*, 2022, **800**, 139681.
28 E. C. Njagi, H. Huang, L. Stafford, H. Genuino, H. M. Galindo, J. B. Collins, G. E. Hoag and S. L. Suib, *Langmuir*, 2011, **27**, 264–271.
29 M. A. J. Kouhbanani, N. Beheshtkhoo, S. Taghizadeh, A. M. Amani and V. Alimardani, *Adv. Nat. Sci. Nanosci. Nanotechnol.*, 2019, **10**, 015007.
30 S. Kamilah, C. Soh, A. Azzura, A. Rahman and M. Shamsuddin, *Malaysian J. Anal. Sci.*, 2018, **22**, 768–774.
31 H. Chen, G. Zhang, W. Zhang and W. Gao, *RSC Adv.*, 2023, **13**, 11450–11456.
32 P. Postolache, V. Petrescu, D. D. Dumitrascu, C. Rimbu, N. Vrînceanu and C. R. Cipaian, *Chem. Eng. Commun.*, 2016, **203**, 649–659.
33 M. Yuan, C. Nan, Y. Yang, G. Sun, H. Li and S. Ma, *ACS Omega*, 2017, **2**, 4269–4277.
34 G. Wang, Y. Yang, X. Xu, S. Zhang, Z. Yang, Z. Cheng, J. Xian, T. Li, Y. Pu, W. Zhou, G. Xiang and Z. Pu, *Molecules*, 2023, **28**, 1–18.
35 K. Shameli, M. Bin Ahmad, A. Zamanian, P. Sangpour, P. Shabanzadeh, Y. Abdollahi and M. Zargar, *Int. J. Nanomed.*, 2012, **7**, 5603–5610.
36 K. Jyoti, M. Baunthiyal and A. Singh, *J. Radiat. Res. Appl. Sci.*, 2016, **9**, 217–227.
37 S. P. Vinay, Udayabhanu, H. N. Sumedha, G. Nagaraju, S. Harishkumar and N. Chandrasekhar, *Appl. Organomet. Chem.*, 2020, **34**, e5830.
38 E. Gürsoy, G. B. Vonbun-Feldbauer and R. H. Meißner, *J. Phys. Chem. Lett.*, 2023, **14**, 6800–6807.
39 B. Guan, D. Ding, L. Wang, J. Wu and R. Xiong, *Mater. Res. Express*, 2017, **4**, 056103.
40 M. E. Compeán-Jasso, F. Ruiz, J. R. Martínez and A. Herrera-Gómez, *Mater. Lett.*, 2008, **62**, 4248–4250.
41 S. T. Gentry, S. F. Kendra and M. W. Bezpalko, *J. Phys. Chem. C*, 2011, **115**, 12736–12741.
42 M. Ganguly, A. Pal and T. Pal, *J. Phys. Chem. C*, 2012, **116**, 9265–9273.
43 Z. Markova, P. Novak, J. Kaslik, P. Plachtova, M. Brazdova, D. Jancula, K. M. Siskova, L. Machala, B. Marsalek, R. Zboril and R. Varma, *ACS Sustain. Chem. Eng.*, 2014, **2**, 1674–1680.
44 V. A. Lavrenko, A. I. Malyshevskaya, L. I. Kuznetsova, V. F. Litvinenko and V. N. Pavlikov, *Powder Metall. Met. Ceram.*, 2006, **45**, 476–480.
45 C. R. Lohani, J. M. Kim and K. H. Lee, *Bioorganic Med. Chem. Lett.*, 2009, **19**, 6069–6073.
46 C. R. Lohani and K. H. Lee, *Sensor. Actuator. B Chem.*, 2010, **143**, 649–654.
47 M. Ganguly, S. Dib, U. Kurien, R. B. Rangel-Alvarado, Y. Miyahara and P. A. Ariya, *J. Phys. Chem. C*, 2018, **122**, 18690–18704.
48 M. Ganguly, S. Dib and P. A. Ariya, *Sci. Rep.*, 2018, **8**, 1–10.
49 J. Liu, Q. Zhang, W. Xue, H. Zhang, Y. Bai, L. Wu, Z. Zhai and G. Jin, *Nanomaterials*, 2019, **9**, 1294.
50 Z. Wang, Y. Huang, D. Lv, G. Jiang, F. Zhang and A. Song, *Green Chem. Lett. Rev.*, 2019, **12**, 197–207.
51 J. R. Lakowicz, *Anal. Biochem.*, 2005, **337**, 171–194.
52 S. Mamta, G. Mainak and S. Priyanka, *Nanoscale Adv.*, 2024, **6**, 4545–4566.

53 R. Giri, *Spectrochim. Acta, Part A*, 2004, **60**, 757–763.
54 S. P. J. Namal Senanayake, *J. Funct. Foods*, 2013, **5**, 1529–1541.
55 A. R. Vilchis-Nestor, V. Sánchez-Mendieta, M. A. Camacho-López, R. M. Gómez-Espinosa, M. A. Camacho-López and J. A. Arenas-Alatorre, *Mater. Lett.*, 2008, **62**, 3103–3105.
56 N. Muthusamy, P. Kanniah, P. Vijayakumar, U. Murugan, D. S. Raj and U. Sankaran, *J. Inorg. Organomet. Polym. Mater.*, 2021, **31**, 4693–4709.
57 M. Ganguly, A. Pal, Y. Negishi and T. Pal, *Chem.–A Eur. J.*, 2012, **18**, 15845–15855.